PCCP

ROYAL SOCIETY OF CHEMISTRY

PAPER

Cite this: *Phys. Chem. Chem. Phys.*, 2022, **24**, 20249

Benchmark *ab initio* potential energy surface mapping of the F + CH_3NH_2 reaction

Tímea Szűcs and Gábor Czakó *

Received 1st July 2022,
Accepted 2nd August 2022

DOI: 10.1039/d2cp03006c

rsc.li/pccp

This electronic structure study reveals four exothermic and two endothermic reaction pathways of the F + CH_3NH_2 system: the barrierless hydrogen abstraction from the methyl/amino group (HF + CH_2NH_2/CH_3NH), amino/methyl substitution (NH_2 + CH_3F and CH_3 + NH_2F) and hydrogen substitution from the two functional groups (H + CH_2FNH_2/CH_3NHF). The benchmark classical and adiabatic energies are obtained using a high-accuracy composite *ab initio* approach, where the gold-standard explicitly-correlated coupled cluster method (CCSD(T)-F12b) is applied with the correlation-consistent polarized valence quintuple-zeta F12 basis set (cc-pV5Z-F12) and further additive energy contributions. Considering indispensable post-(T) correlation, core correlation, scalar relativistic, spin–orbit and harmonic zero-point energy corrections, the obtained global minimum of the potential energy surface is the post-reaction $CH_2NH_2\cdots HF$ complex in the product channel. Although each substitution pathway has a high barrier, the energies of amino-substitution and methyl-hydrogen-substitution products are below the energy of the reactants, as well as the submerged-barrier hydrogen-abstraction pathways.

I. Introduction

The F + H_2 reaction is one of the most widely studied fundamental chemical processes beyond the H + H_2 system.[1–6] Unlike H + H_2, F + H_2 involves a 'heavy' atom, making its electronic-structure description more challenging. Nevertheless, a high-level *ab initio* potential energy surface (PES) was developed for the F + H_2 system in the 1990s,[3] enabling quantum scattering computations to provide deep insight into the atomic-level state-to-state dynamics. In 2013 Schaefer and co-workers[7] asked the question, "What comes after F + H_2?". Of course, the reactions of F with H_2O,[8] NH_3,[9] CH_4,[10,11] and C_2H_6[12,13] are more complex due to the larger number of electrons and nuclei making both the electronic structure and nuclear motion parts more challenging. In the past few decades, significant progress has been achieved on these systems as well, advancing our fundamental knowledge on polyatomic reactivity.[8–13] Thus, the next step forward could be to replace the molecular reactant with a molecule that has two functional groups, such as, for example, CH_3OH and CH_3NH_2. Theoretical research toward this direction has also been started, especially in the case of the F + CH_3OH reaction.[14–17]

In the present study we focus on the F + CH_3NH_2 system following the early experiments[18,19] on the F + CH_3ND_2 reaction, which measured the HF/DF vibrational and rotational distributions and the theoretical study of Schaefer and co-workers,[7] which characterized the two hydrogen-abstraction pathways. What comes after the previous work on the title reaction? First, it is important to note that the previous computations only considered the H-abstraction channels, whereas our recent studies on the F/Cl/Br/I/OH + C_2H_6[20,21] and Cl + CH_3NH_2/CH_3CN[22,23] reactions revealed several other channels, such as hydrogen and methyl substitution, for the reactions of C_2H_6, and the picture is even more complex in the cases of CH_3NH_2 and CH_3CN. Thus, in the present study, we plan to characterize all the possible, chemically relevant pathways of the title reaction, thereby providing new qualitative insights into the mechanisms of the F + CH_3NH_2 process. Furthermore, knowing the challenging electronic structure of the reactions of the fluorine atom, we plan to use the highest technically feasible level of theory to achieve sub-chemical accuracy for the relative energies of the stationary points. In 2013 Schaefer and co-workers[7] used the standard CCSD(T) method with the aug-cc-pV*n*Z [*n* = 2(D), 3(T), 4(Q)] basis sets; however, this previous work did not consider accelerating the basis-set convergence using the explicitly-correlated CCSD(T)-F12b method, electron correlation beyond CCSD(T), and the effects of core correlation, scalar relativity, and spin–orbit coupling. In the present study, we take all of the above-mentioned corrections into account, thereby anchoring the relative energies of the stationary points of the title reaction. These new benchmark data will guide future PES developments and reaction-dynamics simulations, whose results may be

MTA-SZTE Lendület Computational Reaction Dynamics Research Group, Interdisciplinary Excellence Centre and Department of Physical Chemistry and Materials Science, Institute of Chemistry, University of Szeged, Rerrich Béla tér 1, Szeged H-6720, Hungary. E-mail: gczako@chem.u-szeged.hu

directly compared with experiments. In Section II we describe the details of the composite *ab initio* computations; the results are presented and discussed in Section III; and the paper ends with our summary and conclusions in Section IV.

II. Computational details

During the characterization of the potential energy surface, we build upon previous work[7,22] and chemical intuition to identify the important stationary points of the F + CH_3NH_2 reaction. We use the restricted open-shell second-order Møller–Plesset perturbation theory (RMP2)[24] and the correlation-consistent aug-cc-pVDZ basis set[25] to determine the primary geometries, energies and harmonic vibrational frequencies. In order to refine the structures, further optimizations are performed using the restricted open-shell Hartree–Fock (ROHF)-based unrestricted explicitly correlated coupled-cluster singles, doubles and perturbative triples (CCSD(T)-F12b)[26] method accompanied with the aug-cc-pVDZ basis set. To increase the accuracy, based on these structures thus obtained, CCSD(T)-F12b/aug-cc-pVTZ geometry and frequency computations are performed as well as further single-point CCSD(T)-F12b computations with the aug-cc-pVQZ and cc-pV*n*Z-F12 [n = 2(D), 3(T), 4(Q), 5] basis sets[27] being executed by keeping the minima and saddle points fixed at the CCSD(T)-F12b/aug-cc-pVTZ geometries.

The most accurate benchmark classical relative energies are obtained in this work using the following expression:

$$\Delta E_{\text{classical}} = \text{CCSD(T)-F12b/cc-pV5Z-F12} + \delta[\text{CCSDT}] + \delta[\text{CCSDT(Q)}] + \Delta_{\text{core}} + \Delta_{\text{rel}} + \Delta_{\text{SO}}, \quad (1)$$

where δ[CCSDT], δ[CCSDT(Q)], Δ_{core}, Δ_{rel} and Δ_{SO} are the additive energy corrections detailed below, which are taken into account with single-point-energy computations at the most-accurate CCSD(T)-F12b/aug-cc-pVTZ geometries.

To acquire the post-(T) correlation energy contributions, unrestricted CCSD(T),[28] CCSDT[29] and CCSDT(Q)[30] computations – using the unrestricted Hartree–Fock (UHF) reference and the aug-cc-pVDZ basis set – are performed using the MRCC program suite[31,32] interfaced to MOLPRO.[33] The corrections are calculated as follows:

$$\delta[\text{CCSDT}] = \Delta E(\text{CCSDT/aug-cc-pVDZ}) - \Delta E(\text{CCSD(T)/aug-cc-pVDZ}), \quad (2)$$

$$\delta[\text{CCSDT(Q)}] = \Delta E(\text{CCSDT(Q)/aug-cc-pVDZ}) - \Delta E(\text{CCSDT/aug-cc-pVDZ}). \quad (3)$$

During the computational procedures the frozen core (FC) approach is used, where only the valence electrons are correlated. However, the all-electron (AE) method correlates the $1s^2$ electrons as well in the case of the C, N and F atoms. The difference between the energies obtained using these two concepts at the CCSD(T)-F12b/cc-pCVTZ-F12 level of theory[26,34] provides the core (core–core and core–valence) electron correlation correction:

$$\Delta_{\text{core}} = \Delta E(\text{AE-CCSD(T)-F12b/cc-pCVTZ-F12}) - \Delta E(\text{FC-CCSD(T)-F12b/cc-pCVTZ-F12}). \quad (4)$$

Using the second-order Douglas–Kroll (DK)[35] relativistic energies – computed at the AE-CCSD(T)/aug-cc-pwCVTZ-DK level of theory[28,36] – the scalar relativistic effect is defined as follows:

$$\Delta_{\text{rel}} = \Delta E(\text{DK-AE-CCSD(T)/aug-cc-pwCVTZ-DK}) - \Delta E(\text{AE-CCSD(T)/aug-cc-pwCVTZ}). \quad (5)$$

The interacting-states approach[37] is used with the Davidson-corrected[38] all-electron multi-reference configuration interaction[39] (MRCI+Q) method to determine the spin–orbit (SO) coupling effect. The aug-cc-pwCVTZ basis set[40] is used and an active space of 5 electrons in the 3 spatial 2p-like fluorine orbitals is applied. During the SO computations the diagonal elements of the 6 × 6 SO matrix are replaced by the Davidson-corrected MRCI energies and the SO eigenstates are obtained by diagonalizing this matrix. Subtracting the non-SO ground-state (non-SO_1) energy from the SO ground-state (SO_1) energy gives the Δ_{SO} correction:

$$\Delta_{\text{SO}} = \text{SO}_1\text{(MRCI+Q/aug-cc-pwCVTZ)} - \text{non-SO}_1\text{(MRCI+Q/aug-cc-pwCVTZ)}. \quad (6)$$

Considering the zero-point energy contributions (Δ_{ZPE}) obtained at the CCSD(T)-F12b/aug-cc-pVTZ level of theory, the vibrationally adiabatic relative energies are determined as follows:

$$\Delta E_{\text{adiabatic}} = \text{CCSD(T)-F12b/cc-pV5Z-F12} + \delta[\text{CCSDT}] + \delta[\text{CCSDT(Q)}] + \Delta_{\text{core}} + \Delta_{\text{rel}} + \Delta_{\text{SO}} + \Delta_{\text{ZPE}}. \quad (7)$$

The computations detailed above are accomplished using the MOLPRO program package.[33]

III. Results and discussion

1. Benchmark energies and geometries

Our computations reveal the main pathways of the F + CH_3NH_2 reaction. When a fluorine atom attacks a hydrogen atom at either the methyl or amino group, this gives two different abstraction channels, leading to the HF + CH_2NH_2 and to HF + CH_3NH products, respectively. During a reaction, a hydrogen atom can be substituted as well, resulting in the H + CH_2FNH_2 or H + CH_3NHF products for the two functional groups. The processes for which the attacking atom substitutes NH_2 (leading to CH_3F + NH_2) or CH_3 (leading to NH_2F + CH_3) are also investigated in this study. To illustrate the determined benchmark energies of the stationary points relative to the reactants, we use the schematic energy diagram of the seven examined reaction pathways in Fig. 1. The classical(adiabatic) relative energy values are derived from eqn (1) and (7) and are presented in Table 1. The key structural parameters obtained at the three different levels of theory are shown in Fig. 2, which provide useful information for identifying the stationary structures of the PES.

The most exothermic mechanisms are the hydrogen abstraction (HA) reactions, with $\Delta E(\Delta H_0)$ = −41.26(−44.12) kcal mol^{-1} in the case of hydrogen transfer from the methyl group and

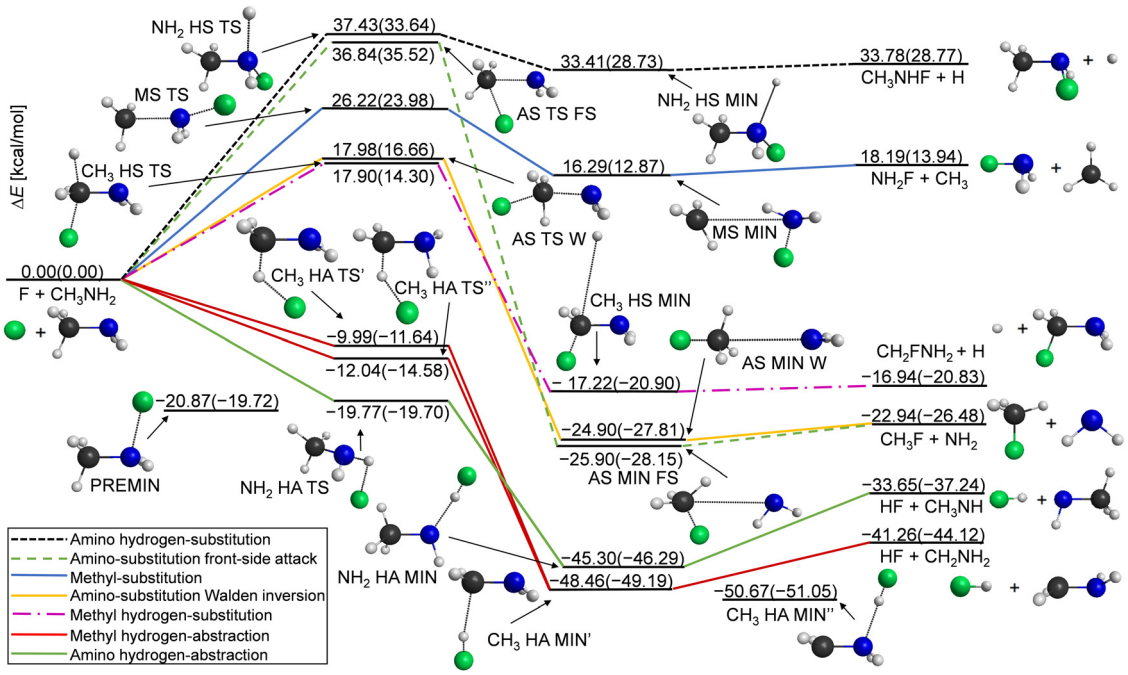

Fig. 1 Schematic energy diagram of the $F(^2P_{3/2})$ + CH_3NH_2 reaction's potential energy surface, illustrating the CCSD(T)-F12b/aug-cc-pVTZ optimized geometries and benchmark classical(adiabatic) relative energies. PREMIN is not connected because it can perform an important role in more pathways.

Table 1 Benchmark classical and adiabatic energies with auxiliary energy contributions relative to reactants (kcal mol^{-1}), obtained at CCSD(T)-F12b/aug-cc-pVTZ geometries

Stationary points	CCSD(T)-F12b cc-pV5Z-F12[a]	δ[T][b]	δ[(Q)][c]	Δ_{core}[d]	Δ_{rel}[e]	Δ_{SO}[f]	Classical[g]	Δ_{ZPE}[h]	Adiabatic[i]
PREMIN	−20.61	−0.20	−0.46	−0.08	+0.11	+0.37	−20.87	+1.15	−19.72
CH_3 HA TS′	−9.24	−0.66	−0.52	−0.12	+0.20	+0.34	−9.99	−1.65	−11.64
CH_3 HA TS″	−11.39	−0.54	−0.46	−0.14	+0.14	+0.36	−12.04	−2.54	−14.58
NH_2 HA TS	−19.31	−0.40	−0.44	−0.08	+0.10	+0.36	−19.77	+0.07	−19.70
AS TS W	18.37	−0.60	−0.62	+0.47	+0.01	+0.36	17.98	−1.32	16.66
AS TS FS	37.72	−1.08	−0.69	+0.53	+0.00	+0.37	36.84	−1.32	35.52
MS TS	26.77	−0.75	−0.63	+0.49	−0.04	+0.37	26.22	−2.24	23.98
CH_3 HS TS	18.30	−0.42	−0.58	+0.12	+0.11	+0.37	17.90	−3.60	14.30
NH_2 HS TS	37.53	−0.28	−0.52	+0.33	+0.01	+0.37	37.43	−3.79	33.64
CH_3 HA MIN′	−48.51	−0.08	−0.22	−0.22	+0.20	+0.37	−48.46	−0.73	−49.19
CH_3 HA MIN″	−50.80	−0.06	−0.19	−0.19	+0.20	+0.37	−50.67	−0.38	−51.05
NH_2 HA MIN	−45.50	−0.16	−0.12	−0.01	+0.13	+0.37	−45.30	−0.99	−46.29
AS MIN W	−25.42	−0.17	−0.05	+0.30	+0.07	+0.37	−24.90	−2.91	−27.81
AS MIN FS	−26.40	−0.17	−0.05	+0.28	+0.08	+0.37	−25.90	−2.24	−28.15
MS MIN	16.03	−0.18	−0.25	+0.28	+0.04	+0.37	16.29	−3.42	12.87
CH_3 HS MIN	−17.69	+0.07	−0.19	+0.06	+0.17	+0.37	−17.22	−3.68	−20.90
NH_2 HS MIN	33.10	+0.00	−0.34	+0.23	+0.05	+0.37	33.41	−4.68	28.73
CH_3NHF + H	33.47	+0.00	−0.34	+0.23	+0.05	+0.37	33.78	−5.00	28.77
NH_2F + CH_3	17.91	−0.16	−0.24	+0.28	+0.04	+0.37	18.19	−4.25	13.94
CH_2FNH_2 + H	−17.42	+0.07	−0.19	+0.06	+0.17	+0.37	−16.94	−3.89	−20.83
CH_3F + NH_2	−23.47	−0.17	−0.04	+0.29	+0.07	+0.37	−22.94	−3.53	−26.48
HF + CH_3NH	−33.92	−0.16	−0.11	+0.07	+0.10	+0.37	−33.65	−3.59	−37.24
HF + CH_2NH_2	−41.38	−0.07	−0.18	−0.19	+0.20	+0.37	−41.26	−2.86	−44.12
CH_4 + NHF	3.77	−0.38	−0.19	+0.35	−0.05	+0.37	3.87	−3.84	0.03
NH_3 + CH_2F	−29.96	−0.15	−0.11	+0.07	+0.15	+0.36	−29.65	−3.12	−32.77

[a] CCSD(T)-F12b/cc-pV5Z-F12 relative energies. [b] CCSDT – CCSD(T) obtained using the aug-cc-pVDZ basis set. [c] CCSDT(Q) – CCSDT obtained using the aug-cc-pVDZ basis set. [d] Core correlation correction obtained as the difference between all-electron and frozen-core CCSD(T)-F12b/cc-pCVTZ-F12 relative energies. [e] Scalar relativistic effect obtained as the difference between DK-AE-CCSD(T)/aug-cc-pwCVTZ-DK and AE-CCSD(T)/aug-cc-pwCVTZ relative energies. [f] Spin–orbit (SO) corrections obtained as the difference between the SO and non-SO ground-state MRCI+Q/aug-cc-pwCVTZ relative energies. [g] Benchmark classical relative energies obtained as CCSD(T)-F12b/cc-pV5Z-F12 relative energies + δ[T] (*b*) + δ[(Q)] (*c*) + Δ_{core} (*d*) + Δ_{rel} (*e*) + Δ_{SO} (*f*). [h] Zero-point energy (ZPE) corrections obtained at CCSD(T)-F12b/aug-cc-pVTZ. [i] Benchmark adiabatic relative energies obtained as classical relative energies (*g*) + Δ_{ZPE} (*h*).

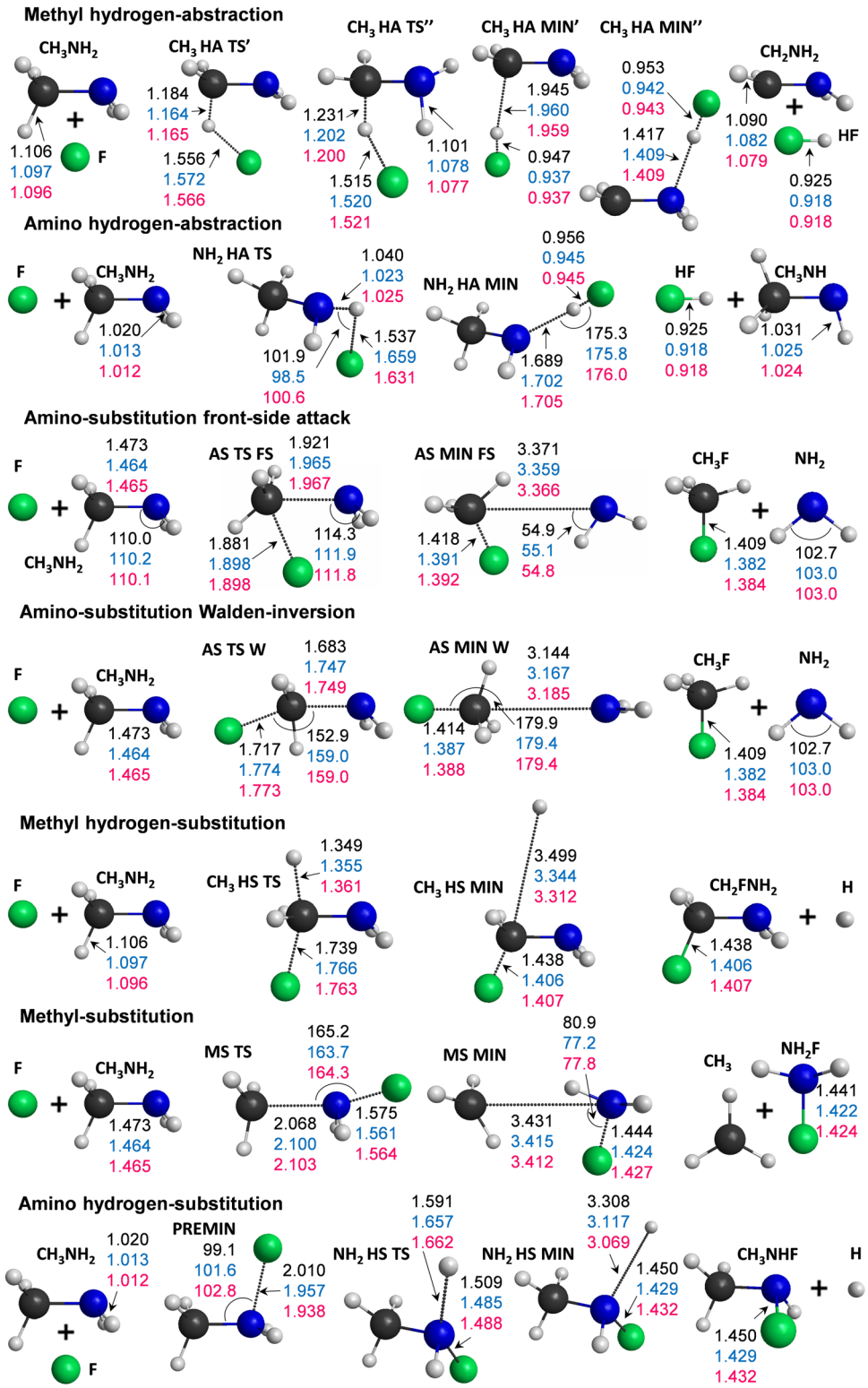

Fig. 2 Optimized geometries of the reactants, stationary-points and products, obtained at the CCSD(T)-F12b/aug-cc-pVTZ level of theory with the characteristic distances (Å) and angles (degree) at three levels of theory: MP2/aug-cc-pVDZ (black), CCSD(T)-F12b/aug-cc-pVDZ (blue) and CCSD(T)-F12b/aug-cc-pVTZ (red).

$\Delta E(\Delta H_0) = -33.65(-37.24)$ kcal mol^{-1} for HA from the amino group. These are followed by the substitution pathways as can be seen in Fig. 1. We found that the CH_3 HA MIN″ structure in the product channel is the global minimum of the PES, where the formed HF binds to the nitrogen atom through a 1.409 Å N···H distance. We present two transition states in the methyl

hydrogen-abstraction channel, where the CH_3 HA TS′ has very similar geometrical and energetic parameters to the structure reported by Feng *et al.*,[7] but the classical(adiabatic) relative energy is more negative by 2.05(2.94) kcal mol^{-1} in the case of TS″. The TS′ and TS″ structures differ in bond lengths by a few hundredths of an ångström and in angles, mainly the plane of the C–N–H atoms relative to the plane of the C–H–F atoms. In the entrance channel a reactant-like pre-reaction complex with a substantial dissociation energy ($D_e(D_0)$ = 20.87(19.72) kcal mol^{-1}) is obtained with a C–N–F angle of 102.8°.

Amino substitution (AS) and methyl-hydrogen substitution (CH_3 HS) are thermodynamically favored like the hydrogen abstractions; however, these substitutions are kinetically not preferred. We could identify front-side attack (FS) and Walden-inversion (W) mechanisms in the case of amino-substitution, where the former has a higher barrier (with 18.86 kcal mol^{-1}) as expected. The classical relative energies of the AS MIN FS and AS MIN W structures in the product channel differ by 1 kcal mol^{-1}, which is in accordance with the very similar lengths of the C–N (3.366/3.185 Å) and C–F (1.392/1.388 Å) bonds. The dipole-polarized-atom force-stabilized CH_3 HS MIN complex has the lowest dissociation energy, $D_e(D_0)$ = 0.28(0.07) kcal mol^{-1}, among the product-like complexes.

The most endothermic pathway is hydrogen substitution from the amino group, and it has the highest barrier. The exit-channel minimum of this process is quite shallow, like in the other HS pathway. The methyl substitution is endothermic as well ($\Delta E(\Delta H_0)$ = 18.19(13.94) kcal mol^{-1}), but it has a lower relative energy than the above-mentioned NH_2 HS channel ($\Delta E(\Delta H_0)$ = 33.78(28.77) kcal mol^{-1}).

2. Convergence of the relative energies

Depending on the level of theory and the basis sets, the convergence of the relative energies is investigated. To compare the MP2 and CCSD(T)-F12b methods, the difference between the relative energies calculated using the same aug-cc-pVDZ basis set can be a guide. The average absolute difference between the results is 0.80 kcal mol^{-1}, but as shown in Table 2, in some cases the MP2 method can seriously overestimate or underestimate the CCSD(T)-F12b relative energies. An example of the former is the barrier height of AS TS W (by 2.5 kcal mol^{-1}) and the latter occurs in the case of PREMIN (by 6.3 kcal mol^{-1}) or the hydrogen-substitution channels (by 3.9–5.0 kcal mol^{-1}). We can conclude that the CCSD(T)-F12b method is needed to achieve chemical accuracy, where the uncertainty is under 1 kcal mol^{-1}.

Furthermore, this study reveals the basis-set effect of the results determined using the CCSD(T)-F12b method, comparing the aug-cc-pV*n*Z (*n* = D, T, Q) and the cc-pV*n*Z-F12 (*n* = D, T, Q, 5) basis sets. In Fig. 3 the relative energies, which are obtained using the above basis sets, are presented relative to the CCSD(T)-F12b/cc-pV5Z-F12 data. In the case of the aug-cc-pVDZ and aug-cc-pVTZ basis sets, the geometry optimizations are carried out, whereas in the other cases single-point computations are performed at the CCSD(T)-F12b/aug-cc-pVTZ geometries. With the increasing basis set, the average absolute deviations between the CCSD(T)-F12b/aug-cc-pV*n*Z

Table 2 Classical energies relative to reactants (kcal mol^{-1}), obtained at MP2/aug-cc-pVDZ and CCSD(T)-F12b with the aug-cc-pV*n*Z (*n* = D, T, Q) and cc-pV*n*Z-F12 basis sets (*n* = D, T, Q, 5). The CCSD(T)-F12b/aug-cc-pVQZ and CCSD(T)-F12b/cc-pV*n*Z-F12 (*n* = D-5) energies are obtained at the CCSD(T)-F12b/aug-cc-pVTZ geometries

	MP2	CCSD(T)-F12b						
Stationary points	aug-cc-pVDZ	aug-cc-pVDZ	aug-cc-pVTZ	aug-cc-pVQZ	cc-pVDZ-F12	cc-pVTZ-F12	cc-pVQZ-F12	cc-pV5Z-F12
PREMIN	−27.63	−21.31	−20.63	−20.69	−20.39	−20.26	−20.54	−20.61
CH_3 HA TS′	−7.33	−9.14	−9.39	−9.38	−8.07	−9.00	−9.21	−9.24
CH_3 HA TS″	−11.59	−11.45	−11.44	−11.52	−10.25	−11.10	−11.33	−11.39
NH_2 HA TS	−17.30	−18.61	−19.38	−19.40	−18.04	−19.07	−19.27	−19.31
AS TS W	21.28	18.81	18.26	18.27	19.52	18.62	18.41	18.37
AS TS FS	39.88	38.19	37.53	37.66	38.77	37.93	37.76	37.72
MS TS	28.89	27.04	26.73	26.72	27.55	27.00	26.84	26.77
CH_3 HS TS	15.37	18.57	18.30	18.22	19.68	18.67	18.38	18.30
NH_2 HS TS	37.45	37.18	37.45	37.48	38.30	37.77	37.60	37.53
CH_3 HA MIN′	−50.54	−48.76	−48.61	−48.68	−47.64	−48.20	−48.44	−48.51
CH_3 HA MIN″	−53.07	−51.01	−50.93	−50.99	−49.89	−50.49	−50.74	−50.80
NH_2 HA MIN	−46.19	−45.80	−45.62	−45.67	−44.92	−45.28	−45.45	−45.50
AS MIN W	−25.23	−25.62	−25.48	−25.51	−24.91	−25.20	−25.39	−25.42
AS MIN FS	−26.20	−26.62	−26.50	−26.50	−25.85	−26.19	−26.37	−26.40
MS MIN	16.33	16.09	16.00	15.98	16.71	16.25	16.09	16.03
CH_3 HS MIN	−23.20	−18.36	−17.71	−17.79	−16.95	−17.39	−17.64	−17.69
NH_2 HS MIN	28.86	32.54	33.04	33.07	33.71	33.34	33.17	33.10
CH_3NHF + H	29.10	32.97	33.41	33.40	33.98	33.73	33.61	33.47
NH_2F + CH_3	18.45	18.26	18.01	17.89	18.54	18.13	17.96	17.91
CH_2FNH_2 + H	−23.03	−18.03	−17.44	−17.54	−16.77	−17.07	−17.28	−17.42
CH_3F + NH_2	−22.83	−23.45	−23.46	−23.54	−22.94	−23.25	−23.43	−23.47
HF + CH_3NH	−34.16	−33.77	−33.80	−33.98	−33.46	−33.72	−33.87	−33.92
HF + CH_2NH_2	−42.75	−41.02	−41.19	−41.45	−40.58	−41.06	−41.32	−41.38
CH_4 + NHF	6.31	4.04	3.87	3.79	4.07	3.88	3.80	3.77
NH_3 + CH_2F	−29.71	−29.77	−29.89	−30.05	−29.16	−29.65	−29.92	−29.96

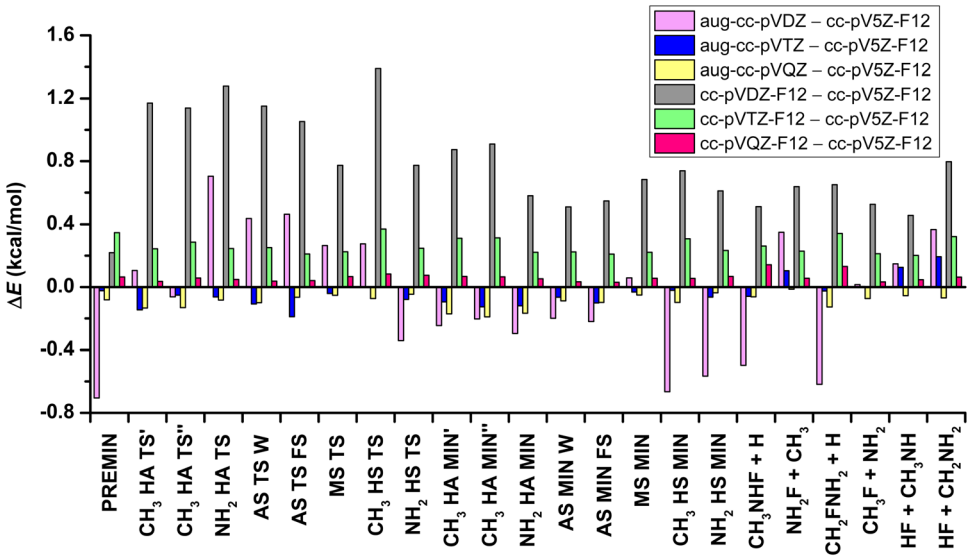

Fig. 3 Difference between the relative energies of the stationary points and products, obtained at the CCSD(T)-F12b level of theory with the aug-cc-pV*n*Z (*n* = D, T, Q) and the cc-pV*n*Z-F12 (*n* = D, T, Q) basis sets compared with the cc-pV5Z-F12 basis set.

and corresponding CCSD(T)-F12b/cc-pV*n*Z-F12 relative energies are decreasing, as 0.80 (*n* = D), 0.29 (*n* = T) and 0.15 (*n* = Q) kcal mol^{-1}. If the results that are achieved using the cc-pV5Z-F12 basis set – used for benchmark values – are examined, as opposed to the results obtained with the mentioned other basis sets, we can establish that the root-mean-square deviation (RMSD) is less for the comparison of aug-cc-pVDZ and cc-pV5Z-F12 (RMSD = 0.37 kcal mol^{-1}), than cc-pVDZ-F12 *vs.* cc-pV5Z-F12 (RMSD = 0.82 kcal mol^{-1}). The inference is similar in the case of the aVTZ – V5Z-F12 and the VTZ-F12 – V5Z-F12 differences, where RMSDs are 0.09 and 0.26 kcal mol^{-1}, respectively. The VQZ-F12 – V5Z-F12 difference is the least, with RMSD = 0.07 kcal mol^{-1}. Thus, the CCSD(T)-F12b/cc-pV5Z-F12 relative energies are clearly basis-set-converged within 0.1 kcal mol^{-1}.

3. Energy contributions

One of the goals of this electronic-structure study is to achieve subchemical accuracy in the relative energies of the characterized structures, thus auxiliary energy corrections must be computed. As we can read from Table 1, the post-CCSD(T) corrections are negative contributions with a few exceptions. The four cases, where δ[CCSDT] is not negative, occur for the hydrogen-substitution exit-channel complexes and products. All of the absolute post-CCSD(T) corrections are in the range of 0.00 to 1.08 kcal mol^{-1} in the case of δ[CCSDT] and go from 0.04 to 0.69 kcal mol^{-1} for δ[CCSDT(Q)], showing that these effects are not negligible. The largest post-(T) correlation effects are found for PREMIN and the TSs, which may have slight multi-reference characters as the T_1 diagnostic[41] values between 0.02 and 0.05 also show. Nevertheless, we think that the neglected post-(Q) effects must be small, and the present correlation treatment is converged within about 0.1–0.2 kcal mol^{-1}, even for the TSs. For the exit-channel complexes and products the T_1 values are always below 0.02, indicating that the use of single-reference wave functions is clearly adequate in these cases.

The sum of the energy contributions of the core correlation and scalar relativistic effect is in the range of −0.02 to 0.52 kcal mol^{-1}. These corrections play the most significant role in the case of the functional-group-substitution pathways, the finding of which is supported by the fact that $\Delta_{core} + \Delta_{rel}$ = 0.52 kcal mol^{-1} for the AS TS FS, whereas this value is only −0.01 kcal mol^{-1} for the CH_3 HA TS″. As this latter value shows, for the stationary points and products of the hydrogen-abstraction channels, these effects almost cancel each other.

The relativistic spin–orbit (SO) interactions in halogen atoms such as F may cause energy lowering in open-shell systems, and we have to take them into account in order to achieve chemical accuracy. The non-relativistic ^{2}P ground state (non-SO) of the fluorine atom splits to the ground $^2P_{3/2}$ state, with a lower energy by 1/3ε, and to the excited $^2P_{1/2}$ state (SO_3), with a higher energy by 2/3ε regarding the non-SO state, where ε is the SO splitting between the $^2P_{3/2}$ and $^2P_{1/2}$ states. While the F atom approaches the CH_3NH_2 molecule, the former fourfold degenerate state splits into two twofold degenerate states: the SO ground (SO_1) and SO excited (SO_2) states. Furthermore, three twofold degenerate states form as a result of the splitting of the non-SO ground state, resulting in a non-SO ground (non-SO_1) and two non-SO excited states (non-SO_2 and non-SO_3). The potential energy curves of these six states, for the cases where the fluorine atom approaches the methylamine from seven different directions, are investigated and detailed in Subsection III.4. The SO-coupling-instigated energy decrease of the F atom is calculated as the difference between the asymptotic limits of the SO_1 and non-SO_1 potential energies. In general, this results in a SO correction of 0.37 kcal mol^{-1}, whereas Δ_{SO} is 0.34/0.36 kcal mol^{-1} for hydrogen-abstraction transition states and AS TS W, the effect of which will be further discussed below.

The energy contribution values, as mentioned above, do not exceed 1 kcal mol^{-1} (one exception), whereas the effect of the relative-energy shifting caused by the harmonic zero-point

energy (ZPE) is more significant. For the reactant-like PREMIN and NH_2 HA TS the ZPE correction is positive, but in all other cases Δ_{ZPE} is negative. The absolute correction for the products is larger than for the TS or MIN complexes, due to the decrease in the number of vibrational degrees of freedom in the product channels, or, for example, for the H-substitution pathways, due to the replacement of the high-frequency C–H/N–H stretching modes with lower-frequency C–F/N–F bonds. For example, the NH_2 HS TS has a -3.79 kcal mol^{-1} ZPE correction, the NH_2 HS MIN has -4.68 kcal mol^{-1}, and this effect is -5.00 kcal mol^{-1} for the CH_3NHF + H products.

Considering of all the energy corrections mentioned so far, we can compare the computed benchmark adiabatic relative energies (obtained using eqn (7)) with the experimental data, which are provided by the Active Thermochemical Tables (ATcT).[42] The 0 K reaction enthalpy is determined by extracting the enthalpy of formation from the ATcT database for the reactants and products for the following three reaction pathways: hydrogen abstraction from the methyl group (CH_3 HA) and from the amino group (NH_2 HA) and for amino substitution (AS), where $\Delta H_0 = -43.98 \pm 0.11$, -37.22 ± 0.12 and -26.10 ± 0.08 kcal mol^{-1}, respectively. By comparison, the present benchmark *ab initio* ΔH_0 values are -44.12, -37.24 and -26.48 kcal mol^{-1} in order. In the case of NH_2 HA, the agreement between the experimental and theoretical data is outstanding, where the deviation is only 0.02 kcal mol^{-1}. Although for the other two pathways the differences are not within the ATcT uncertainty determined *via* Gaussian propagation law, they are nevertheless well below the 1 kcal mol^{-1} chemical accuracy.

4. Potential energy curves of the F···CH_3NH_2 system

As described in the previous subsection, three SO and three non-SO states play key roles in describing the F···CH_3NH_2 interaction. Representative potential energy curves, relative to the ground non-SO_1 asymptotic limit, are shown in Fig. 4A, where the fluorine atom approaches the methylamine molecule perpendicularly to the C–N bond (CN2). At the reaction asymptote, where the inter-fragment distance is large, the previously-mentioned SO correction of about 0.37 kcal mol^{-1} can be seen as the difference between the energy of SO_1 and non-SO_1, but as the reactants approach each other, this effect drops to zero. Fig. 4C shows this SO_1 – non-SO_1 difference for the seven approaching directions as indicated in Fig. 4D. The decrease in energy is not steep; it starts around at 4 Å and lasts until about 2 Å, but when the fluorine atom attacks methylamine from the side of the amino group (CN1, N1, N3), the decay starts at around 5 Å.

To investigate the reactive SO_1 state corresponding to the different orientations of separation, we illustrate the potential curves of this state in Fig. 4B. The van der Waals wells are shallow with depths of 0.2–0.5 kcal mol^{-1} in the region of 3.0–3.5 Å, when fluorine approaches the C or N atom from the hydrogen (C2, N2), the C atom along the line of the C–N bond (C1) or the C–N bond perpendicularly (CN2). The wells are deeper for the cases where F approaches methylamine from the

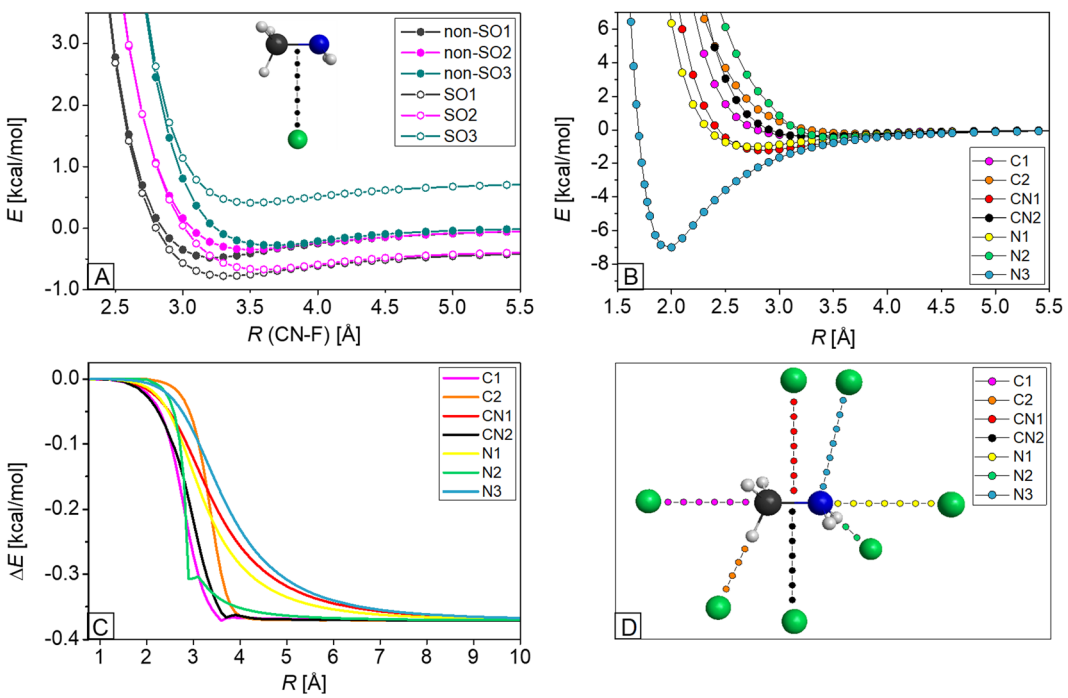

Fig. 4 (A) Potential energy curves of six states in the case of CN2 as indicated in panel D; (B and C) distance-dependence of the energy of the SO_1 state (B) and $E(SO_1) - E(\text{non-}SO_1)$ (C) for the seven orientations indicated in panel D; and (D) seven different separation orientations of the F atom and methylamine, which is kept frozen in its equilibrium geometry, where fluorine approaches the C atom in line with the C–N bond (C1) or in line with a C–H bond (C2), the C–N bond perpendicularly from two sites (CN1 and CN2), the N atom in line with the C–N bond (N1), in line with the N–H bond (N2), or from the same orientation as in PREMIN (N3). Potential energies are obtained at the MRCI+Q/aug-cc-pwCVTZ level of theory.

more polar amino group in line with (N1) or perpendicularly to (CN1) the C–N bond, and are the deepest (−7.0 kcal mol^{-1} at 2 Å distance) when the angle of the approach is equal to the C–N–F angle obtained in PREMIN (N3). Here it is important to note that MRCI+Q seriously underestimates the well depth of PREMIN as the benchmark value is 20.87 kcal mol^{-1} (see Fig. 1) and the geometry effect corresponding to fixed *vs.* relaxed CH_3NH_2 is only 0.1 kcal mol^{-1}. These findings indicate that dynamical electron correlation, even beyond single and double excitations, is important for describing the F$\cdots$$CH_3NH_2$ interaction. To further support this conclusion, we report that the PREMIN complex is unbound at the ROHF level, and CCSD-F12b underestimates the CCSD(T)-F12b well depth by 3.7 kcal mol^{-1}. These extremely large correlation effects are not unprecedented as the barrier height of the F + CH_4 reaction is 9.41, 1.80, and 0.55 kcal mol^{-1} at the ROHF, CCSD, and CCSD(T) levels of theory, respectively.[10]

5. Comparing the F + CH_3NH_2 and the Cl + CH_3NH_2 reactions

As we published in our previous work,[22] in the reaction of Cl + CH_3NH_2 there are six reaction channels, as in the title reaction: two hydrogen-abstraction pathways from the two functional groups and are four substitution pathways, where the halogen atom substitutes the amino/methyl group or one hydrogen of these. When methylamine reacts with the fluorine atom, the reaction channels are more exothermic than in the case of reaction with chlorine; however, in both cases the CH_3 HA products have the lowest relative energy and the NH_2 HS products have the highest. The global minimum of the vibrationally adiabatic PES belongs to the CH_3 HA MIN″ complex for the two reactions (−51.05/−15.56 kcal mol^{-1} for F/Cl + methylamine), but while in case of the F + CH_3NH_2 system it is the classical minimum as well (−50.67 kcal mol^{-1}), in the case of Cl + CH_3NH_2 classically the global minimum belongs to the PREMIN structure (−15.30 kcal mol^{-1}). We have found that the CH_3F/CH_3Cl + NH_2 and CH_2ClNH_2 + H products can be formed by both Walden-inversion and front-side attack mechanisms; however, we have not found the front-side attack pathway for the formation of the CH_2FNH_2 + H products. These two channels are exothermic in the title reaction, but in the case of Cl + CH_3NH_2 they are endothermic.

The two additional kinetically hindered product channels are also investigated in the title reaction, where two bonds are required to break and form, leading to NH_3 + CH_2F and CH_4 + NHF. The products of the former channel have a $\Delta E(\Delta H_0)$ = −29.65(−32.77) kcal mol^{-1} relative energy and those of the latter have a $\Delta E(\Delta H_0)$ = 3.87(0.03) kcal mol^{-1}, whereas the corresponding values for the Cl + CH_3NH_2 system are −3.70(−8.20) and 14.24(9.82) kcal mol^{-1}, respectively.[22] In both reactions, the exothermic NH_3 formation is thermodynamically competitive with H-abstractions; however, the former may have a much higher barrier due to the two bond cleavages required to form the NH_3 + CH_2F/CH_2Cl products.

The calculated SO interactions, which lower the asymptote of the reactants by 0.84 kcal mol^{-1} and 0.37 kcal mol^{-1} for the chlorine and fluorine reactions, respectively, show good agreement with the measured SO splittings (ε_{expt})[43] of these atoms, as $\varepsilon_{expt}/3$ = 0.84 (Cl) kcal mol^{-1} and 0.39 (F) kcal mol^{-1}. Considering the different separation orientations of the reactants, it can be seen for both systems that the deepest van der Waals wells of the potential energy curves occur when the halogen atom approaches the amino group of methylamine with the angle of C–N–Cl/F obtained at the PREMIN geometry. The depth is shallower if the F/Cl atom attacks the molecule at the side of the hydrogens or at the methyl group in line with the C–N bond. The distance dependence of the SO – non-SO ground-state energy difference for the different approaching orientations is quite similar for the two systems.

IV. Summary and conclusions

In addition to the previously-studied[7] exothermic hydrogen-abstraction pathways of the F + CH_3NH_2 reaction, the hydrogen and functional-group substitutions are investigated as well in the present theoretical study. Transition states and post-reaction complexes are identified in all the reaction channels. The methyl-hydrogen abstraction has the lowest adiabatic energy among the exothermic channels (ΔH_0 = −44.12 kcal mol^{-1}), which is followed by amino-hydrogen abstraction, amino-substitution, and methyl-hydrogen-substitution with reaction enthalpies of −37.24, −26.48, and −20.83 kcal mol^{-1}, in ascending energy order. Amino substitution can proceed *via* Walden-inversion and front-side-attack mechanisms, where the latter has a higher classical barrier height by 18.86 kcal mol^{-1}, although the energies of the post-reaction minima are close to each other. The two thermodynamically unfavored endothermic pathways are methyl substitution and amino-hydrogen substitution. The global minimum of the potential energy surface corresponds to the complex CH_3 HA MIN″ in the product channel, where the formed HF binds to the N atom of the CH_2NH_2 fragment. A pre-reaction minimum has been found in the entrance channel, which has a deeper energy (−19.72 kcal mol^{-1} adiabatically) than all saddle points, and thus it may play an important steering role in all the reaction pathways.

The above-indicated subchemically accurate benchmark energy values are obtained by taking into account further energy contributions besides the CCSD(T)-F12b/cc-pV5Z-F12 single-point energies obtained at the CCSD(T)-F12b/aug-cc-pVTZ geometries. As we have already seen in the case of the reaction between chlorine and methylamine,[22] the zero-point energy correction is the most significant among the energy contributions determined by us. By considering the post-(T) correlation (which mainly affects the energy of the TS structures and often by more than 1 kcal mol^{-1}), the core electron correlation and scalar relativistic effects (which are usually negligible to reach chemical accuracy but are often needed if subchemical accuracy is desired), and the SO correction of about 0.37 kcal mol^{-1}, we are able to achieve excellent agreement with the experimental results for the three product channels, where data are available in the ATcT database.

This study provides guidance for the development of a global analytical *ab initio* potential energy surface required for the first-principles investigation of reaction dynamics, thereby enabling a comparison with the results obtained *via* experiments, and gaining deeper atomic insight into the mechanisms of the F + CH_3NH_2 reaction.

Conflicts of interest

There are no conflicts of interest to declare.

Acknowledgements

We thank the National Research, Development and Innovation Office – NKFIH, K-125317; the Ministry of Human Capacities, Hungary grant 20391-3/2018/FEKUSTRAT; Project no. TKP2021-NVA-19, provided by the Ministry of Innovation and Technology of Hungary from the National Research, Development and Innovation Fund, financed under the TKP2021-NVA funding scheme; and the Momentum (Lendület) Program of the Hungarian Academy of Sciences for financial support.

References

1 G. C. Schatz and A. Kuppermann, *J. Chem. Phys.*, 1975, **62**, 2502.
2 G. C. Schatz, J. M. Bowman and A. Kuppermann, *J. Chem. Phys.*, 1975, **63**, 674.
3 K. Stark and H.-J. Werner, *J. Chem. Phys.*, 1996, **104**, 6515.
4 D. E. Manolopoulos, *J. Chem. Soc., Faraday Trans.*, 1997, **93**, 673.
5 L. Che, Z. Ren, X. Wang, W. Dong, D. Dai, X. Wang, D. H. Zhang, X. Yang, L. Sheng, G. Li, H.-J. Werner, F. Lique and M. H. Alexander, *Science*, 2007, **317**, 1061.
6 W. Dong, C. Xiao, T. Wang, D. Dai, X. Yang and D. H. Zhang, *Science*, 2010, **327**, 1501.
7 H. Feng, W. Sun, Y. Xie and H. F. Schaefer III, *Chem. Phys. Chem.*, 2013, **14**, 896.
8 B. Fu, X. Shan, D. H. Zhang and D. C. Clary, *Chem. Soc. Rev.*, 2017, **46**, 7625.
9 L. Tian, Y. Zhu, H. Song and M. Yang, *Phys. Chem. Chem. Phys.*, 2019, **21**, 11385.
10 G. Czakó, B. C. Shepler, B. J. Braams and J. M. Bowman, *J. Chem. Phys.*, 2009, **130**, 084301.
11 J. F. Castillo, F. J. Aoiz, L. Banares, E. Martinez-Nunez, A. Fernandez-Ramos and S. Vazquez, *J. Phys. Chem. A*, 2005, **109**, 8459.
12 J. Espinosa-Garcia, J. C. Corchado, M. Garcia-Chamorro and C. Rangel, *Phys. Chem. Chem. Phys.*, 2018, **20**, 19860.
13 D. Papp and G. Czakó, *J. Chem. Phys.*, 2020, **153**, 064305.
14 M. L. Weichman, J. A. DeVine, M. C. Babin, J. Li, L. Guo, J. Ma, H. Guo and D. M. Neumark, *Nat. Chem.*, 2017, **9**, 950.
15 D. Lu, J. Li and H. Guo, *Chem. Sci.*, 2019, **10**, 7994.
16 D. Lu and J. Li, *Theor. Chem. Acc.*, 2020, **139**, 157.
17 M. Zhang, Y. Zhu and J. Li, *Chin. J. Chem. Phys.*, 2022, **35**, 153.
18 R. G. Macdonald, J. J. Sloan and P. T. Wassell, *Chem. Phys.*, 1979, **41**, 201.
19 S. Wategaonkar and D. W. Setser, *J. Chem. Phys.*, 1987, **86**, 4477.
20 D. Papp, B. Gruber and G. Czakó, *Phys. Chem. Chem. Phys.*, 2019, **21**, 396.
21 B. Gruber and G. Czakó, *Phys. Chem. Chem. Phys.*, 2020, **22**, 14560.
22 T. Szűcs and G. Czakó, *Phys. Chem. Chem. Phys.*, 2021, **23**, 10347.
23 P. Tóth, T. Szűcs and G. Czakó, *J. Phys. Chem. A*, 2022, **126**, 2802.
24 R. D. Amos, J. S. Andrews, N. C. Handy and P. J. Knowles, *Chem. Phys. Lett.*, 1991, **185**, 256.
25 T. H. Dunning, Jr., *J. Chem. Phys.*, 1989, **90**, 1007.
26 G. Knizia, T. B. Adler and H.-J. Werner, *J. Chem. Phys.*, 2009, **130**, 054104.
27 K. A. Peterson, T. B. Adler and H.-J. Werner, *J. Chem. Phys.*, 2008, **128**, 084102.
28 K. Raghavachari, G. W. Trucks, J. A. Pople and M. Head-Gordon, *Chem. Phys. Lett.*, 1989, **157**, 479.
29 J. Noga and R. J. Bartlett, *J. Chem. Phys.*, 1987, **86**, 7041.
30 M. Kállay and J. Gauss, *J. Chem. Phys.*, 2005, **123**, 214105.
31 M. Kállay, P. R. Nagy, D. Mester, Z. Rolik, G. Samu, J. Csontos, J. Csóka, B. P. Szabó, L. Gyevi-Nagy, B. Hégely, *et al.* MRCC, a quantum chemical program suite, see **www.mrcc.hu**.
32 M. Kállay, P. R. Nagy, D. Mester, Z. Rolik, G. Samu, J. Csontos, J. Csóka, P. B. Szabó, L. Gyevi-Nagy and B. Hégely, *et al.*, *J. Chem. Phys.*, 2020, **152**, 074107.
33 H.-J. Werner, P. J. Knowles, G. Knizia, F. R. Manby, M. Schütz, *et al.*, *Molpro, version 2015.1, a package of ab initio programs*, see **https://www.molpro.net**.
34 J. G. Hill, S. Mazumder and K. A. Peterson, *J. Chem. Phys.*, 2010, **132**, 054108.
35 M. Douglas and N. M. Kroll, *Ann. Phys.*, 1974, **82**, 89.
36 W. A. de Jong, R. J. Harrison and D. A. Dixon, *J. Chem. Phys.*, 2001, **114**, 48.
37 A. Berning, M. Schweizer, H.-J. Werner, P. J. Knowles and P. Palmieri, *Mol. Phys.*, 2000, **98**, 1823.
38 S. R. Langhoff and E. R. Davidson, *Int. J. Quantum Chem.*, 1974, **8**, 61.
39 K. R. Shamasundar, G. Knizia and H.-J. Werner, *J. Chem. Phys.*, 2011, **135**, 054101.
40 K. A. Peterson and T. H. Dunning, Jr., *J. Chem. Phys.*, 2002, **117**, 10548.
41 T. J. Lee and P. R. Taylor, *Int. J. Quantum Chem.*, 1989, **S23**, 199.
42 B. Ruscic and D. H. Bross, Active Thermochemical Tables (ATcT) values based on ver. 1.122r of the Thermochemical Network (2021); available at **ATcT.anl.gov**.
43 The National Institute of Standards and Technology (NIST), Handbook of Basic Atomic Spectroscopic Data, **https://www.nist.gov/pml/data/handbook/**.